

Analytical and numerical stability analysis of Soret-driven convection in an horizontal porous layer

M.C. Charrier-Mojtabi^a, B. Elhajjar^b and A. Mojtabi^b

a) P.H.A.S.E, E.A. 3028, UFR PCA, University Paul Sabatier, 118 route de Narbonne, 31062, Toulouse Cedex, France

b) IMFT, UMR CNRS/INP/UPS N°5502, UFR MIG, University Paul Sabatier, 118 route de Narbonne, 31062, Toulouse Cedex, France.

E. mail: cmojtabi@cict.fr

Keywords: Soret-driven Convection, stability, porous medium, binary fluid

Abstract

We present an analytical and numerical stability analysis of Soret-driven convection in a porous cavity saturated by a binary fluid. Both the mechanical equilibrium solution and the mono-cellular flow obtained for particular ranges of the physical parameters of the problem are considered. The porous cavity, bounded by horizontal infinite or finite boundaries, is heated from below or from above. The two horizontal plates are maintained at different constant temperatures while no mass flux is imposed. The influence of the governing parameters and more particularly the role of the separation ratio, ψ , characterizing the Soret effect and the normalized porosity, ε , are investigated theoretically and numerically.

From the linear stability analysis, we find that the equilibrium solution loses its stability via a stationary bifurcation or a Hopf bifurcation depending on the separation ratio and the

normalized porosity of the medium. The role of the porosity is important, when it decreases, the stability of the equilibrium solution is reinforced.

For a cell heated from below, the equilibrium solution loses its stability via a stationary bifurcation when the separation ratio $\psi > \psi_0(Le, \varepsilon)$, while for $\psi < \psi_0(Le, \varepsilon)$, it loses stability via a Hopf subcritical bifurcation. The oscillatory solution is unstable and becomes stationary.

For a cell heated from above, the equilibrium solution is linearly stable if $\psi > 0$, while a stationary or an oscillatory bifurcation occurs if $\psi < 0$.

The results obtained from the linear stability analysis are widely corroborated by direct 2D numerical simulations.

In the case of long-wave disturbances, for $\psi < 0$ and for ψ higher than a particular value called ψ_{mono} , we observe that the mono-cellular flow leads to a separation of the species between the two ends of the cell. First, we determined the velocity, temperature and concentration fields analytically for mono-cellular flow. Then we studied the stability of this flow. For a cell heated from below and for $\psi > \psi_{mono}$ the mono-cellular flow loses stability via a Hopf bifurcation. As the Rayleigh number increases, the resulting oscillatory solution evolves to a stationary multicellular flow. For a cell heated from above and $\psi < 0$, the mono-cellular flow remains linearly stable. We verified numerically that this problem admits other stable multicellular stationary solutions for this range of parameters

I. INTRODUCTION

Double-diffusive convection in a porous medium due to temperature and concentration gradients has been widely studied because of its numerous fundamental and industrial applications. Some examples of interest are the migration of moisture in fibrous insulation,

the transport of contaminants in saturated soil, drying processes or solute transfer in the mushy layer during the solidification of binary alloys. A review of recent developments and publications in this field is given by Nield and Bejan¹ and by Ingham and Pop². The onset of thermosolutal convection was first studied by Nield³. The cross coupling between thermal diffusion and solutal diffusion was not taken into account in these studies. The Soret effect cannot be neglected in many physical processes. It has been well known for more than half a century that, without the Soret effect, convection is initiated when the Rayleigh number Ra , based on the permeability of the porous medium, exceeds the value $Ra_c = 4\pi^2$. In a binary fluid, due to the imposed temperature gradient, the Soret effect induces a vertical concentration gradient that drastically modifies the density gradient and therefore the conditions for the onset of convection.

There are numerous studies on double-diffusive convection and, in some of them, the Soret effect is taken into account. The boundary conditions are either fixed temperatures and concentrations or imposed heat and mass fluxes. A compilation of most of the pertinent information given by recent research in double-diffusive convection in porous media can be found in the Porous Media handbook edited by Vafai⁴. For the studies concerning the Soret-driven convection in fluid we can refer to Platten and Legros⁵ and to Batiste et al.⁶. For binary mixtures in a porous medium we can refer to Brand and Steinberg^{7,8}, to Bahloul et al.⁹ and to Bourich et al.^{10,11}. These studies were motivated by the fact that, in many cases, the oscillatory instabilities occur as a second bifurcation as in the case of single component fluids while, for a binary mixture in a porous cell heated from below with negative separation ratio, the first bifurcation corresponds to oscillatory instability. Brand and Steinberg also point out that, with the Soret effect, it is possible to have oscillatory instability for a cell heated from above. They present an amplitude equation for an oscillatory convective instability in a porous medium cell saturated by binary mixture. Brand et al.¹² derive an amplitude equation

for a binary fluid in a porous medium in the vicinity of the intersection point between the stationary and oscillatory curves. The slow spatial modulations are also included in the amplitude equation near this codimension-2 bifurcation point. Schöpf¹³, using realistic boundary conditions for the first time to our knowledge, compared the onset of convection in a binary mixture saturating a porous medium with a binary mixture in a narrow cell. He showed that the fluid flows in a narrow cell and in porous medium become identical when the height-to-width ratio becomes infinite (Hele-Shaw limit). He used the same mathematical formulation previously used by the Brand and Steinberg group. The influence of the porosity was ignored, so that Schöpf¹³ results are correct only for a normalized porosity equal to one. He numerically solved the linear stability equations relative to the onset of Soret-driven convection in the case of a porous medium and in the case of a narrow box. Ouarzazi and Bois¹⁴ also used the same Brand and Steinberg group mathematical formulation to study the convective instability of a fluid mixture in a porous medium in the case where the prescribed temperature gradient varies periodically in time. They found that the subharmonic instability was always the first instability for the phenomenon. The neighbourhood of the polycritical point was also studied in the case of small force frequency.

Nield and Bejan¹ and Quintard and Whitaker¹⁵ showed that the porosity appears in the transient term coefficient, in the species conservation equation, while in the previous work of Brand and Steinberg^{7, 8} and of Schöpf¹³, the coefficient was taken equal to one. In our opinion, this is due to the inadequate physical formulation used by these authors as it was well demonstrated in the book of Nield and Bejan¹.

The role of the porosity is taken into account in many recent contributions for similar problem but for boundary conditions different from that used in the present work. Bahloul et al.⁹ and Bourich et al.^{10, 11} studied the stability of the flow in a horizontal layer in the case of double diffusive convection with or without Soret effect. They considered boundary

conditions with uniform heat flux applied on the horizontal walls and impermeable adiabatic vertical walls. They found a general analytical solution valid for these two cases. Their work includes an analytical model for finite amplitude convection and numerical results allowing the determination of the first Hopf bifurcation. For finite amplitude convection, a comparison is made to illustrate the difference between double diffusive convection and Soret-driven convection in terms of Nusselt and Sherwood numbers.

Bourich et al.¹⁰ presented an analytical and numerical study of Soret-driven convection in horizontal porous layer heated from below by an uniform constant flux. Using the parallel flow approximation, they determined the thresholds for subcritical and stationary convection, depending on the governing parameters. Their numerical solution for the full governing equations is in good agreement with the analytical solution. These two works were extended by Bourich et al.¹¹ considering not only a shallow horizontal porous cavity but also a shallow enclosure with clear binary fluid. The relation between a saturated porous medium cell and a binary fluid was obtained using the Brinkman-Hazen-Darcy model in its transient form. The critical Rayleigh numbers for the onset of oscillatory and stationary convection were determined explicitly as functions of the governing parameters for infinite layers and bounded boxes. At the onset of instability, they found that the wave-number is equal to zero while for our boundary conditions the wave-number is equal to zero only in a particular range of the separation ratio. They also showed the dependency of critical parameters on the normalized porosity.

The onset of oscillatory binary fluid convection in a two dimensional domain with realistic boundary conditions on all boundaries is determined as function of the fluid parameters and the aspect ratio of the container by O. Batiste et al.⁶. The critical parameters were obtained for two particular values of Lewis, Prandlt, and separation ratio numbers as function of the aspect ratio. The choice of these critical parameters was motivated by the

experiments associated to $^3\text{He}/^4\text{He}$ and water ethanol mixture. Sovran et al.¹⁶ in their study related to the onset of Soret-driven convection in an infinite porous layer also considered the effect of porosity.

The existence of multiple solutions and the influence of the Soret effect on convection in a horizontal porous domain under cross temperature and concentration gradients are discussed by Bennacer et al.¹⁷. Mojtabi et al.¹⁸ give a linear stability analysis of free convection in a binary mixture with variable Soret coefficient. Labrosse¹⁹ presents a detailed analysis of steady state regimes in a thermogravitational column for a binary liquid with variable Soret coefficient. Charrier-Mojtabi et al.²⁰ consider the influence of the direction of vibration on the stability threshold of two-dimensional Soret-driven convection in an infinite layer filled with a binary mixture, which can be heated from below or from above. They concluded that the vertical vibration has stabilizing effect while the horizontal vibration has destabilizing effect on the onset of convection. The case associated with the absence of vibrations corresponds to the present problem. Recently, Ryzhkov et al.²¹ extended the theoretical framework for describing multicomponent mixtures with Soret effect. Three-dimensional numerical modeling of Soret-driven convection in a cubic cell filled with a binary mixture of water (90%) and isopropanol (10%) was performed by Shevtsova et al.²². These authors²³ observed instability occurring in this binary fluid with negative Soret coefficient and for a cubic cell heated from above.

In a porous medium, the use of Darcy's law simplifies the hydrodynamic equations and, in most cases, makes an analytical determination of the critical thermal Rayleigh number Ra_c possible, even for the realistic case of impervious boundary conditions (no mass flux across the boundaries).

The aim of our work is to study the linear and nonlinear stability of the equilibrium solution and the mono-cellular flow that appears, under certain conditions, in a horizontal

porous layer filled by a binary fluid and heated from below or above. The Soret effect is taken into account and the influence of both the separation ratio ψ and the normalized porosity ε is studied. In a first part, in the case of realistic boundary conditions, an analytical solution giving the critical Rayleigh number and wave-number is obtained for both infinite and confined cells. With these realistic boundary conditions the critical wave-number at the onset of convection is not constant, contrary to the case of the unrealistic boundary conditions used previously (prescribed concentration on the boundaries, see Brand and Steinberg^{7, 8} and Nield and Bejan¹). The critical Rayleigh number of the Hopf bifurcation varies with ψ and ε , whereas, for stationary bifurcation, it only depends on ψ . In a second part, an analytical model based on the parallel flow approximation is proposed in order to describe the mono-cellular flow obtained at the onset of convection. Thus the critical Rayleigh number corresponding to the loss of stability of mono-cellular flow is predicted. The study is completed by numerical simulations of the full governing equations.

II . Mathematical formulation

We consider a rectangular cavity of aspect ratio $A = L/H$ where L is the width in the horizontal x direction and H is the height of the cavity in the vertical z direction (the gravity acceleration is: $\mathbf{g} = -g \mathbf{k}$). The cavity is filled with a porous medium saturated by a binary fluid and the Soret effect is taken into account. The impermeable horizontal walls ($z = 0, z = H$) are maintained at different and constant temperatures T_1 for $z = 0$ and T_2 for $z = H$, with $T_1 < T_2$ or $T_1 > T_2$. The vertical walls ($x = 0, x=L$) are impermeable and adiabatic. All the boundaries are assumed rigid.

We consider an isotropic and homogeneous porous medium. We assume that Darcy's law is valid and that the Oberbeck-Boussinesq approximation is applicable: the thermophysical

properties of the binary fluid are considered constant except the density in the buoyancy term which varies linearly with the local temperature and mass fraction:

$$\rho = \rho_0(1 - \beta_T(T - T_i) - \beta_c(C - C_i)) \quad (1)$$

where β_T and β_c are respectively the thermal and mass expansion coefficients of the binary fluid, T is the dimensional temperature and C the mass fraction of the denser component (T_i and C_i correspond to the reference state). We also use the other standard assumptions (local thermal equilibrium, negligible viscous dissipation, etc.).

The resulting dimensionless governing conservation equations for mass, momentum, energy and chemical species, with the Soret effect taken into account are:

$$\begin{cases} \nabla \cdot \mathbf{V} = 0 \\ \mathbf{V} = -\nabla P + Ra(T + \psi C)\mathbf{k} \\ \frac{\partial T}{\partial t} + \mathbf{V} \cdot \nabla T = \nabla^2 T \\ \varepsilon \frac{\partial C}{\partial t} + \mathbf{V} \cdot \nabla C = \frac{1}{Le} (\nabla^2 C - \nabla^2 T) \end{cases} \quad (2)$$

The reference scales are H for the length, $H^2 / (\lambda^* / (\rho c)^*)$ for the time (where λ^* and $(\rho c)^*$ are respectively the effective thermal conductivity and heat capacity of the porous medium), a/H for the velocity with $a = \lambda^* / (\rho c)_f$ (a is the effective thermal diffusivity), $\Delta T = T_1 - T_2$ for the temperature and $\Delta C = -\Delta T C_i (1 - C_i) D_T / D^*$ for the mass fraction, where C_i, D_T, D^* are respectively the initial or reference mass fraction, the thermo-diffusion and the mass-diffusion coefficient of the denser component.

The dimensionless boundary conditions are:

$$\begin{aligned} T = 1 \text{ for } z = 0; \quad T = 0 \text{ for } z = 1; \quad \frac{\partial T}{\partial x} = \frac{\partial C}{\partial x} = 0 \text{ for } x = 0, A, \\ \nabla C \cdot \mathbf{n} = \nabla T \cdot \mathbf{n} \text{ for } z = 0, 1, \quad \mathbf{V} \cdot \mathbf{n} = 0 \quad \forall M \in \partial\Omega \end{aligned} \quad (3)$$

The problem under consideration depends on five non-dimensional parameters: the thermal Rayleigh number, $Ra = K g \beta_T H \Delta T (\rho c)_f / (\lambda^* \nu)$, the separation ratio $\psi = -(\beta_c / \beta_T)(D_T / D^*) C_i (1 - C_i)$, the Lewis number $Le = a / D^*$, the normalized porosity $\varepsilon = \varepsilon^* (\rho c)_f / (\rho c)^*$ (where ε^* is the porosity) and the aspect ratio $A = L / H$.

III. LINEAR STABILITY OF EQUILIBRIUM SOLUTION

A. Onset of Soret-driven convection in an infinite horizontal cell

It is easy to show that there exists a mechanical equilibrium solution characterized by:

$$\mathbf{V} = \mathbf{0}; \quad T_0 = 1 - z; \quad C_0 = C_i + 1/2 - z \quad (4)$$

where C_i is the initial mass fraction.

In order to analyze the stability of this conductive solution, we introduce a vertical velocity component perturbation w , and perturbations of temperature, θ , and concentration, c . We assume that the perturbations (w , θ , c) are small and we obtain the following linearized equations:

$$\begin{cases} \nabla^2 w - Ra \frac{\partial^2}{\partial x^2} (\theta + \psi c) = 0 \\ \frac{\partial \theta}{\partial t} - \nabla^2 \theta = w \\ \varepsilon Le \frac{\partial c}{\partial t} - \nabla^2 (c - \theta) = w Le \end{cases} \quad (5)$$

with the boundary conditions:

$$\begin{aligned} \frac{\partial w}{\partial z} = \frac{\partial c}{\partial x} = \frac{\partial \theta}{\partial x} = 0 \quad \text{for } x = 0 \quad \text{and } x = A \quad \forall z \\ w = \theta = \frac{\partial c}{\partial z} - \frac{\partial \theta}{\partial z} = 0 \quad \text{for } z = 0 \quad \text{and } z = 1 \quad \forall x \end{aligned} \quad (6)$$

For simplicity, we introduce $\eta = c - \theta$, so that (5) reads :

$$\begin{cases} \nabla^2 w - Ra \frac{\partial^2}{\partial x^2} (\theta(1 + \psi) + \psi \eta) = 0 \\ \frac{\partial \theta}{\partial t} - \nabla^2 \theta = w \\ \varepsilon Le \frac{\partial (\theta + \eta)}{\partial t} - \nabla^2 (\eta) = w Le \end{cases} \quad (7)$$

with:

$$\begin{aligned} \frac{\partial w}{\partial z} = \frac{\partial \eta}{\partial x} = \frac{\partial \theta}{\partial x} = 0 \quad \text{for } x = 0 \text{ and } x = A \quad \forall z; \\ w = \theta = \frac{\partial \eta}{\partial z} = 0 \quad \text{for } z = 0 \text{ and } z = 1 \quad \forall x \end{aligned} \quad (8)$$

The perturbation quantities are chosen as follows:

$$(w, \theta, \eta) = (\hat{w}, \hat{\theta}, \hat{\eta}) \exp(ikx + \sigma t) \quad (9)$$

where k is the wave-number in the horizontal direction (\mathbf{ox}) and $I^2 = -1$, and σ is the temporal amplification of the perturbation.

1. Non-realistic boundary conditions

In this part, the porosity is taken into account. But, as in Refs 7-8, idealized boundary conditions are considered for concentration perturbation: $c = 0$, instead of $\partial c / \partial z - \partial \theta / \partial z = 0$ for $z = 0$ and $z = 1 \quad \forall x$.

With the non-realistic boundary conditions, the other authors obtained, for the stationary instability, the following critical Rayleigh number and critical wave number:

$$Ra_{cs} = \frac{4\pi^2}{1 + \psi(1 + Le)} \quad \text{with } k_c = \pi \quad (10)$$

For the oscillatory instability, they obtained the critical parameters given by:

$$Ra_{co} = \frac{4\pi^2(1 + Le)}{(1 + \psi)Le}, \quad k_{co} = \pi, \quad \omega_{co}^2 = \frac{-4\pi^4(1 + \psi + \psi Le(1 + Le))}{(1 + \psi)Le^2} \quad (11)$$

where ω_{co} is the pulsation at the onset of convection.

These results were previously mentioned by Brand and Steinberg group.

When we replace in equations (5):

$$(w, \theta, c) = (w^*, \theta^*, c^*) \sin(\pi z) \exp(Ikx + I\omega t) \quad (12)$$

The linear stability study leads to the homogeneous algebraic system:

$$\begin{bmatrix} k^2 + \pi^2 & -Rak^2 & -\psi Rak^2 \\ -1 & (k^2 + \pi^2 + I\omega) & 0 \\ -Le & -(k^2 + \pi^2) & k^2 + \pi^2 + I\omega \epsilon Le \end{bmatrix} \begin{bmatrix} w^* \\ \theta^* \\ c^* \end{bmatrix} = \begin{bmatrix} 0 \\ 0 \\ 0 \end{bmatrix} \quad (13)$$

The critical parameters for stationary and oscillatory onset of convection are obtained by considering that the real and imaginary parts of the matrix determinant (Eq. 13) are equal to zero. We obtain the same expression as in Ref. (7, 8) for the critical Rayleigh number associated with the stationary bifurcation. For the oscillatory instability, we find the following results mentioned by Nield and Bejan¹ :

$$Ra_{co} = \frac{4\pi^2(1 + \epsilon Le)}{(\epsilon + \psi)Le}, \quad k_{co} = \pi, \quad \omega_{co}^2 = \frac{-4\pi^4(1 + \psi + \epsilon\psi Le(1 + Le))}{(\epsilon + \psi)\epsilon Le^2} \quad (14)$$

and also for the relation between stationary and oscillatory critical Rayleigh number:

$$Ra_{cs} - Ra_{co} = \frac{-4\pi^2(1 + \psi + \epsilon\psi Le(1 + Le))}{(1 + \psi(1 + Le))(\epsilon + \psi)Le} \quad (15)$$

Eq.14 shows that a Hopf bifurcation occurs when:

$$(1 + \psi + \epsilon\psi Le(1 + Le))(\epsilon + \psi) < 0 \quad (16)$$

corresponding to:

$$\psi \in \left[-\epsilon, -\frac{1}{1 + (1 + Le)\epsilon Le} \right] \text{ or } \psi \in \left[-\frac{1}{1 + (1 + Le)\epsilon Le}, -\epsilon \right] \quad (17)$$

We verify that the two roots of Eq.16, $\psi = -\varepsilon$ and $\psi = -1/(1 + (1 + Le)\varepsilon Le)$ are equal for: $\varepsilon = 1/(1 + Le)$ and, in this case: $(1 + \psi + \varepsilon\psi Le(1 + Le))(\varepsilon + \psi) = (1 + \psi(1 + Le))^2 / (1 + Le)$, is therefore always positive, which proves that for $\varepsilon = 1/(1 + Le)$ the problem does not admit a Hopf bifurcation. This situation can be obtained either in the case of a gas saturating an ordinary porous medium or in the case of a binary liquid saturating a medium with very low porosity such as coal ($\varepsilon \in [0.02, 0.12]$). For a binary mixture such as water-ethanol ($Le \approx 100$) saturating a sand porous medium ($\varepsilon \in [0.3, 0.57]$) we verify that the Hopf bifurcation occurs before the stationary one and the polycritical point is defined by $Ra_{cs} - Ra_{co} = 0$ which yields:

$$\omega_{co} = 0, \quad \psi = -\frac{1}{1 + (1 + Le)\varepsilon Le}, \quad Ra_{cs} = Ra_{co} = \frac{4\pi^2(1 + \varepsilon Le + \varepsilon Le^2)}{Le(\varepsilon + \varepsilon Le - 1)} \quad (18)$$

For fixed values of Lewis number and separation ratio and for a cell heated from below, the oscillatory critical Rayleigh number Ra_{co} increases when ε decreases and for a cell heated from above Ra_{co} increases when ε decreases as shown in Fig.1 ($Le=2$) and Fig. 2 ($Le=10$). We show in the next paragraph that we do not observe the same behavior in the case of realistic boundary conditions.

2. Realistic boundary conditions.

Contrary to the eigenvalue problem studied in section III.A.1, the problem with realistic boundary conditions is non-separable and therefore cannot be solved analytically. We developed two procedures to obtain the critical values of (Ra_{cs}, k_{cs}) and $Ra_{co}, k_{co}, \omega_{co}$. The first procedure consists in solving analytically the dispersion equation for stationary transition

to obtain numerically the exact values of the critical parameters and the second one leads to approximate values using the Galerkin method.

a. Stationary transition

In a first part, we focus on steady bifurcation. The realistic boundary conditions considered for the concentration perturbation are:

$$\frac{\partial c}{\partial z} - \frac{\partial \theta}{\partial z} = 0 \quad \text{for } z=0 \text{ and } z=1 \quad \forall x \quad (19)$$

With this, Eq. 7 leads to a sixth-order differential problem that we transform, after a first integration, into the following fourth-order equation:

$$(D^2 - k^2)^2 \hat{\theta} - Rak^2(1 + \psi(1 + Le))\theta = Rak^2\psi(\alpha_1 \sinh(kz) + \alpha_2 \cosh(kz)) \quad (20)$$

where $D = \partial/\partial z$ and α_1 and α_2 are integration constants verifying:

$$\begin{aligned} \hat{\theta} = \hat{\theta}'' = 0 & \quad \text{for } z=0, z=1 \quad \forall x \\ Le\hat{\theta}'(0) + k\alpha_1 = 0 & \quad \text{for } z=0 \quad \forall x \\ Le\hat{\theta}'(1) + k\alpha_1 \cosh(k) + k\alpha_2 \sinh(k) = 0 & \quad \text{for } z=1 \quad \forall x \end{aligned} \quad (21)$$

Equation. 20 is solved as follows: we first determine the algebraic solutions of the characteristic equation associated with Eq. 20:

$$(r^2 - k^2)^2 - Rak^2(1 + \psi + \psi Le) = 0 \quad (22)$$

The general solution of the fourth order ordinary differential equation (Eq. 22) is given as a combination of 4 particular independent functions whose expression depends on the sign of $Ra(1 + \psi + \psi Le)$. These considerations permit us to distinguish 4 regions of the plane (Ra, ψ) . The solution of Eq.20 is the sum of the general solution of the homogeneous associated equation and its particular solution:

$$\frac{-\psi(\alpha_1 \sinh(kz) + \alpha_2 \cosh(kz))}{1 + \psi + Le\psi} \quad (23)$$

The solution obtained depends on six arbitrary constants. When we assume that this general solution verifies the boundary conditions (Eq. 21), we obtain a homogeneous linear algebraic system with six equations and six unknowns corresponding to the six constants. This system has a non-trivial solution if the associated matrix determinant, $\det(Ra(k), k, Le, \psi)$ is equal to zero. The expression of this determinant was obtained using the Maple algebra code. Once we have calculated the determinant, we obtain the relation between the Rayleigh number, the wave-number, the Lewis number and the separation ratio ψ :

$$\begin{aligned} & 2Le k \psi R_2 (1+\psi) \sinh(R_1) \cos(R_2) \cosh(k) + \\ & k^2 (2 (1+\psi)^2 + Le^2 \psi^2) \sinh(R_1) \sinh(k) \sin(R_2) + \\ & Le^2 \psi^2 R_1 R_2 \cosh(R_1) \sinh(k) \cos(R_2) + \\ & 2Le \psi k R_1 (1+\psi) \cosh(R_1) \cosh(k) \sin(R_2) - Le^2 \psi^2 R_1 R_2 \sinh(k) \\ & - 2 Le \psi k (1+\psi) (R_2 \sinh(R_1) + R_1 \sin(R_2)) = 0 \end{aligned}$$

where :

$$Ra_m = Ra\sqrt{(1+\psi+\psi Le)}, \quad R_1 = \sqrt{(k + Ra_m)k}, \quad R_2 = \sqrt{(Ra_m - k)k}$$

We can then determine the exact value of the stationary critical Rayleigh number and the corresponding critical wave-number function of the separation ratio and the Lewis number (Table I).

For: $1 + \psi + \psi Le = 0$, Eq. 20 is solved analytically, using the Maple algebra code. We obtain two possible dispersion equations corresponding to the first and the second bifurcation

$$Ra_1 = f_1(k)(Le + 1)/Le \quad \text{and} \quad Ra_2 = f_2(k)(Le + 1)/Le \quad (24)$$

where:

$$f_1(k) = 8k^2 (e^{3k} + e^{2k} - e^k - 1) / (2k^2 e^k - 2k^2 e^{2k} + 2ke^k + e^k + 2ke^{2k} - e^{2k} - e^{3k} - 1)$$

$$f_2(k) = 8k^2 (e^{3k} - e^{2k} - e^k + 1) / (2k^2 e^k + 2k^2 e^{2k} + 2ke^k + e^k - 2ke^{2k} + e^{2k} - e^{3k} - 1)$$

The first and second dispersion equations lead respectively to:

$$\begin{aligned} Ra_{c_1} &= -12(Le + 1)/Le, \quad k_{c_1} = 0 \quad \text{and} \\ Ra_{c_2} &= -230.4(Le + 1)/Le, \quad k_{c_2} = 3.402 \quad \forall Le \end{aligned} \quad (25)$$

We demonstrate in this case that the line $\psi = -1/(1 + Le)$ is not an asymptote of the curve $Ra_{cs}(\psi)$, as is the case with the non-realistic boundary conditions, but intersects $Ra_{cs}(\psi)$ at $Ra_{cs} = -12(Le + 1)/Le$.

These results were confirmed using the Galerkin method for the perturbation quantities (φ, θ, η) , where φ represents the stream function perturbation:

$$\hat{\varphi} = \sum_{n=1}^N \varphi_n \sin(n\pi z), \quad \hat{\theta} = \sum_{n=1}^N \theta_n \sin(n\pi z), \quad \hat{\eta} = \sum_{n=1}^N \eta_n \cos(n\pi z) \quad (26)$$

In Table I are reported the critical values of Rac_s and kc_s obtained with the exact solution and the Galerkin method, for the stationary bifurcations and for different values of ψ . In Fig.3, 4 and 5, we present the stability diagrams $Ra_c = f(\psi)$ obtained for $Le=2, 10$ and $Le=100$ respectively, (the solid lines are associated to the stationary bifurcation). In Fig.6 the stability diagram $kc_s = f(\psi)$, for $Le=10$, clearly shows the evolution of the critical wave-number versus the separation ratio for stationary bifurcations. For $Rac_s < 0$, $kc_s=0$, $\forall \Psi < 0$ and $Rac_s = 12/(Le\psi)$. If $Rac_s > 0$, $kc_s \rightarrow +\infty$ for $\psi = -1/(1 + Le)$ and decreases progressively to

$$\text{zero for } \psi \in \left[\frac{-1}{Le+1}, \frac{1}{(40/51)Le-1} \right] \text{ For } \psi \geq \frac{1}{(40/51)Le-1}, kc_s=0 \text{ and } Rac_s = 12/(Le\psi).$$

For $\psi > 0$, the denser component moves towards the cooler wall. The pure double diffusive solution is then infinitely linearly stable when the horizontal layer is heated from above ($Ra < 0$) while it loses its stability for critical Rayleigh number smaller than $4\pi^2$ which corresponds to the critical Rayleigh number for the pure thermal problem and for $Ra > 0$.

For $\psi < 0$, the denser component moves towards the warmer wall. For $Ra < 0$, the equilibrium solution is not linearly stable, unlike the pure thermal problem, so we can expect that $Rac_s \rightarrow -\infty$ when $\psi \rightarrow 0^-$. This result was confirmed by our calculations.

For $Ra > 0$ and $(1 + \psi + \psi Le) > 0$, the downward migration of the denser component leads to an increase of the critical Rayleigh number ($Ra_{cs} > 4\pi^2$). For $Ra > 0$ and $(1 + \psi + \psi Le) < 0$, we do not obtain the transition to the stationary convective regime.

b. The case of long-wave disturbances

Although in the general case, the solution of the eigenvalue problem (Eq. 7, 8), can only be obtained numerically, the case of long-wave disturbances (wave-number $k=0$) can be studied analytically.

To study the behavior of long-wave disturbances, one may develop the regular perturbation method with the wavenumber k as a small parameter. In our case, using the Maple algebra code, we expand the determinant in the vicinity of $k=0$ to obtain:

$$\det(Ra(k), k, Le, \psi) = \lambda(Ra, Le, \psi)k^5 + \mu(Ra, Le, \psi)k^7 + o(k^9) \quad (27)$$

where:

$$\lambda(Ra, Le, \psi) = 2Ra(1 + \psi + \psi Le)(RaLe\psi / 12 - 1) \quad (28)$$

The complete expression of $\mu(Ra, Le, \psi)$ is very complicated so it will be given only later and after simplification. When we set the expression corresponding to the order 5 of the determinant development $\lambda(Ra, Le, \psi)$ to zero, it leads to $Ra_{cs} = 12 / \psi Le$ when $k \rightarrow 0$, and when we replace the expression of the critical Rayleigh number in $\mu(Ra, Le, \psi)$, we obtain:

$$\mu(Ra = 12 / Le\psi, Le, \psi) = -\frac{2(1 + \psi(Le + 1))(91Le\psi - 51(1 + \psi(Le + 1)))}{35Le^2\psi^2} \quad (29)$$

For $Ra > 0$, we find the analytical expression:

$$Ra_{cs} = 12 / \psi Le \text{ and } k_{cs} = 0, \text{ for } \psi > \psi_{mono} = 1 / (40Le / 51 - 1) \quad (30)$$

and for $\psi < 0$ and $Ra < 0$, we obtain $Ra_{cs} = 12 / \psi Le$ and $k_c = 0$.

These results (Eq. 30) were also obtained, after some tedious calculations, by Schöpf¹³ using a method similar to that described by Knobloch²⁴.

c. Oscillatory instability

The linear stability equations (7) with the realistic boundary condition (8) are solved using two methods. The first one is the Galerkin method where the perturbations are chosen as Fourier functions and polynomial expansions:

$$(\varphi, \theta, \eta) = \sum_{n=1}^N (\varphi_n \sin(n\pi z), \theta_n \sin(n\pi z), \eta_n \sin(n\pi z)) \exp(ikx + \sigma t) \quad (31)$$

$$(\varphi, \theta, \eta) = \sum_{n=1}^N \left(\varphi_n (1-z)z^n, \theta_n (1-z)z^n, \eta_0 + \eta_n \left(\frac{z}{n+2} - \frac{1}{n+1} \right) z^{n+1} \right) \exp(ikx + \sigma t) \quad (32)$$

The convergence of the critical parameters obtained by these two approximations is similar.

The second method used is a collocation spectral method, Cf. § IV.

The purpose is to find an oscillatory instability ($\sigma = i\omega$) for a Rayleigh number Ra_c smaller than the one at which marginal stability $\sigma = 0$ is observed.

The Maple Software was used for the symbolic calculations of the residue and of the $3N \times 3N$ determinant A . With all the approximations used, the determinant has the following form:

$$\det(A) = R(Ra, k, \omega, \varepsilon, Le, \psi) + I S(Ra, k, \omega, \varepsilon, Le, \psi)$$

where R and S are real polynomial functions of $Ra, k, \omega, \varepsilon, Le, \psi$. The degrees of the variable Ra and k in these functions increase according to the order, N , of truncation. For approximation levels $N=3, 4$ and 5 , the symbolic calculations of the $3N \times 3N$ determinant lead to:

$$\det(A) = F_1(Ra, k, \omega, \varepsilon, Le, \psi) F_2(Ra, k, \omega, \varepsilon, Le, \psi)$$

Then $\det(A) = 0$ implies that the real and imaginary parts of F_1 or F_2 are both equal to 0.

We notice that the frequency ω is a root in the equations $\text{Im}(F_1)=0$ and $\text{Im}(F_2)=0$ and when we

set $\omega=0$ in the equations $\text{Real}(F_1)=0$ and $\text{Real}(F_2)=0$, we obtain, with higher accuracy, the value Ra_{cs} obtained analytically above.

If $\omega \neq 0$, it is not possible to obtain an analytical relation giving $(\text{Ra}_{co}, k_{co}, \omega_{co})$ as functions of $(\varepsilon, \text{Le}, \psi)$. Maple numerical software was used to determine the critical values corresponding to the Hopf bifurcation. The values obtained by this procedure are in good agreement with those obtained by direct numerical simulations using collocation spectral method.

For cell heated from below and for $\psi < 0$, the denser component migrates towards the lower, hot plate, producing a stabilizing effect. In that case, if ψ is smaller than ψ_0 , a function of the Lewis number and the normalized porosity, the first primary bifurcation is a Hopf bifurcation. We note that ψ_0 decreases to zero as Le increases ($\psi_0 = -0.12, -5.7 \cdot 10^{-3}$ and $-5.8 \cdot 10^{-5}$ for Le=2, 10, 100 respectively with $\varepsilon=1/2$). We have determined the critical parameters of the Hopf bifurcation for different values of ε , Le and ψ . Fig. 3 and 4 report (dotted lines) the results for Le=2 and Le=10 for different values of the normalized porosity $\varepsilon=7/10, 1/2, 2/5$. The curves corresponding to Le=100 (Fig.5) are similar to that obtained for Le=10.

The diagram presented in these figures differs significantly from the one obtained in the Rayleigh-Benard problem with a binary fluid subjected to the Soret effect (Platten and Legros⁵). We can also observe that the critical values strongly differ from those obtained in Ref. 7 in which the authors used non-realistic boundary conditions ($c = 0$ for $z = 0$ and $1 \forall x$). The intersection point between the stationary instability and the oscillatory instability curves (codimension-2 bifurcation point) is strongly affected by the porosity factor and differs from our analytical results obtained with non-realistic boundary conditions (Eq. 18). For all (ε, Le) values studied we verified that, for $\psi < 0$ and for $\text{Ra} > 0$, the first primary bifurcation is an oscillatory one.

B. Analytic solution of the onset of stationary Soret-driven convection in confined cavity

Let us consider the stationary stability equations (Eq. 7), but using the stream function formulation :

$$\begin{cases} \nabla^2 \varphi + Ra \frac{\partial}{\partial x} (\theta(1 + \psi) + \psi \eta) = 0 \\ \nabla^2 \theta - \frac{\partial \varphi}{\partial x} = 0 \\ \nabla^2 \eta - Le \frac{\partial \varphi}{\partial x} = 0 \end{cases} \quad (33)$$

By eliminating the stream function, we obtain the fourth order differential problem:

$$\begin{cases} \nabla^4 \theta + Ra \frac{\partial^2}{\partial x^2} (\theta(1 + \psi) + \psi \eta) = 0 \\ \nabla^2 (\eta - Le \theta) = 0 \end{cases} \quad (34)$$

In order to clearly define the problem, it is necessary to add new boundary conditions:

$$\begin{aligned} \theta = \frac{\partial \eta}{\partial z} = 0 \quad \text{for } z = 0 \text{ and } z = 1 \quad \forall x \\ \frac{\partial \eta}{\partial x} = \frac{\partial \theta}{\partial x} = 0 \quad \text{for } x = 0 \text{ and } x = A = \frac{L}{H} \quad \forall z \\ \frac{\partial^2 \theta}{\partial z^2} = 0 \quad \text{for } z = 0 \text{ and } z = 1 \quad \forall x \end{aligned} \quad (35)$$

To solve the problem (Eq.34 and Eq. 35), we introduce $\xi(x, z) = \eta - Le\theta$, so that (Eq. 34) reads :

$$\nabla^2 (\eta - Le\theta) = \nabla^2 (\xi(x, z)) = 0 \quad (36)$$

The solution of this equation is given by:

$$\xi(x, z) = \cos(\gamma x) [B_1 \text{ch}(\gamma z) + B_2 \text{sh}(\gamma z)] \quad (37)$$

where $\gamma = i\pi / A$, B_1 and B_2 are arbitrary constants. Using the boundary conditions:

$$\frac{\partial \eta}{\partial z} - Le \frac{\partial \theta}{\partial z} \Big|_{z=0,1} = -Le \frac{\partial \theta}{\partial z} \Big|_{z=0,1} = \cos(\gamma x) [B_1 \gamma \text{sh}(\gamma z) + B_2 \gamma \text{ch}(\gamma z)] \Big|_{z=0,1} \quad (38)$$

we obtain two additional constraints on θ :

$$\begin{aligned}
Le \frac{\partial \theta}{\partial z} \Big|_{z=0} &= -\gamma B_2 \cos(\gamma x) \\
Le \frac{\partial \theta}{\partial z} \Big|_{z=1} &= -\gamma \cos(\gamma x) [B_1 sh(\gamma) + B_2 ch(\gamma)]
\end{aligned} \tag{39}$$

Taking this result into account, we look for solutions of the form:

$$\begin{aligned}
\theta(x, z) &= \cos(\gamma x) \tilde{\theta}(z) \\
\eta(x, z) &= \cos(\gamma x) \tilde{\eta}(z)
\end{aligned} \tag{40}$$

where $\tilde{\eta}(z) = Le \tilde{\theta}(z) + B_1 ch(\gamma z) + B_2 sh(\gamma z)$ depends on the two arbitrary constants B_1 and B_2 .

The partial differential system (Eq. 34) is then transformed into a fourth-order ordinary differential equation with the unknown function $\tilde{\theta}(z)$:

$$(D^2 - \gamma^2)^2 \tilde{\theta}(z) - \gamma^2 Ra [(1 + \psi + \psi Le) \tilde{\theta}(z) + \psi (B_1 ch(\gamma z) + B_2 sh(\gamma z))] = 0 \tag{41}$$

The boundary conditions (Eq. 39) lead to two equations in $\tilde{\theta}$:

$$\begin{aligned}
Le \frac{\partial \tilde{\theta}}{\partial z} \Big|_{z=0} &= -\gamma B_2 \\
Le \frac{\partial \tilde{\theta}}{\partial z} \Big|_{z=1} &= -\gamma [B_1 sh(\gamma) + B_2 ch(\gamma)]
\end{aligned} \tag{42}$$

and the boundary conditions (Eq. 35) lead to 4 equations in $\tilde{\theta}$

$$\begin{aligned}
\tilde{\theta} &= 0 \text{ for } z = 0 \text{ and } z = 1 \quad \forall x \\
\frac{\partial^2 \tilde{\theta}}{\partial z^2} &= 0 \text{ for } z = 0 \text{ and } z = 1 \quad \forall x
\end{aligned} \tag{43}$$

This new ordinary differential problem (Eq. 41, 42 and 43) is exactly the same as the one we obtained previously for an infinite cell (Eq. 20 and 21), the wave-number k being replaced here by $\gamma = i\pi/A$ where $i \in N^*$ is the number of rolls in the x direction. This analytical study leads to the distinction between three domains:

a) $Ra > 0$ and $-1/(Le+1) < \psi < 1/(40Le/51-1)$. In this case Ra_{cs} and k_{cs} are functions of ψ and are obtained numerically. The particular case $\psi = 0$, leads to $Ra_c = 4\pi^2$ and $k_c = \pi$.

b) $Ra > 0$ and $\psi > 1/(40Le/51-1) \Rightarrow Ra_{cs}(\psi) = 12/\psi Le$ and $k_c(\psi) = 0$.

c) $Ra < 0$ and $\psi < 0$. Here we get $Ra_{cs} = 12/Le\psi$ and $k_c(\psi) = 0$.

IV. LINEAR STABILITY OF MONO-CELLULAR SOLUTION

A. Analytical solution of the mono-cellular flow

For the limit case of a shallow cavity $A \gg 1$, we use the parallel flow approximation (Ouriemi et al.²⁵). The basic flow (subscripted “b”) is then as follows:

$$\mathbf{V} = U_b(z)\hat{\mathbf{e}}_x; \quad T_b(z) = bx + f(z); \quad C_b = mx + g(z) \quad (44)$$

We obtain, by using the assumptions already mentioned and the corresponding boundary conditions, the velocity, temperature and concentration profiles for the stationary solution.

$$\begin{cases} T_b = 1 - z \\ U_b = Ra m \psi (1/2 - z) \\ C_b = mx + (m^2 Ra Le \psi (3z^2 - 2z^3))/12 - z - (m^2 Ra Le \psi)/24 + (1 - mA)/2 \\ m = \pm \sqrt{(10 Le Ra \psi - 120)/(Le Ra \psi)} \end{cases} \quad (45)$$

Two remarks can be made concerning the expression of the parameter m in the concentration field. The expression under the root sign must be positive, which means that $Ra > 12/(Le\psi)$. This value of Ra corresponds to the critical Rayleigh number of the onset of convection obtained in paragraph II. m is negative or positive according to whether the flow is clockwise or anticlockwise and both solutions are possible depending on the initial conditions. A similar result, giving the analytical value of the critical Rayleigh number, was obtained by Bahloul et al.⁹ and by Mamou et al.²⁶ in the case of double diffusive convection.

B. Linear stability analysis of the mono-cellular flow

In order to study the stability of the mono-cellular solution, we introduce and expand the perturbations as $(w, \theta, \eta) = (w(z), \theta(z), \eta(z)) \exp(ikx + \sigma t)$. The new system of linearized equations reads :

$$\begin{cases} (D^2 - k^2)w = -Ra k^2((1 + \psi)\theta + \psi\eta) \\ \sigma\theta - w + Ik\theta U_b = (D^2 - k^2)\theta \\ (\varepsilon\sigma Ik - k^2 U_b)(\eta + \theta) - mDw + Ik w D C_b = Ik(D^2 - k^2)\eta / Le \end{cases} \quad (46)$$

where $D = \partial / \partial z$, k is the horizontal wave-number, $\sigma = \sigma_r + I\sigma_i$ and $I^2 = -1$.

The corresponding boundary conditions are:

$$w = 0, \theta = 0, \frac{\partial \eta}{\partial z} = 0 \quad \text{for } z = 0, 1 \quad (47)$$

The resulting linear problem is solved by means of a fifth-order Galerkin method, using the same functions as mentioned in Eq. 32.

Critical values of the Rayleigh number were obtained for stationary and oscillatory bifurcations. For the values of ψ and Le that we studied, the critical Rayleigh number leading to stationary bifurcation was always higher than the one leading to oscillatory bifurcation. So, in this study, we present mainly the variations of the critical wave-number k_{co2} , the critical Rayleigh number Ra_{co2} and the critical frequency ω_{co2} with ψ . The Lewis number is maintained at $Le = 10$ and the porosity at $\varepsilon = 0.5$. In this case $\psi_{mono} = 0.146$. We determine the critical values Ra_{co2} , k_{co2} and ω_{co2} . The results are illustrated in table II. For a layer heated from below we can note that Ra_{co2} has a maximum for $\psi = 0.33$ whereas k_{co2} admits a minimum for $\psi = 0.44$. The critical frequency always increases with ψ . The

stability study enabled us to define the interval of variation of Ra where the mono-cellular flow remains stable thus making it possible to separate the species of the mixture.

V. NUMERICAL SIMULATIONS

In order to corroborate the results obtained with the linear stability analysis for both the equilibrium solution and the mono-cellular solution, several numerical simulations were carried out. These simulations permitted us to observe the onset of convection, for both cases, at the critical Rayleigh number predicted by the linear theory with good agreement.

The equation system (Eq. 2) with the associated boundary conditions (Eq. 3) was solved numerically using a collocation spectral method, well known for its accuracy and a finite element method (Comsol industrial code) with a rectangular grid system, better suited to the rectangular shape of the cell used. For the spectral method, the time scheme was a second order Adams-Bashforth-Euler backward scheme (Azaïez et al.²⁷). The influence of Le , ε and ψ for different values of Ra was investigated for a cell with aspect ratio $A \geq 10$. We showed that the numerical critical values ($Ra_{cnum}, k_{cnum}, \omega_{cnum}$) obtained for $A \geq 10$, were very close to the analytical ones obtained for an infinite cell. For the collocation method, the spatial resolution was 63×27 and 100×20 collocation points along the horizontal and vertical axes respectively and for Comsol the spatial resolution was 100×20 and 150×30 .

A. Stability of the equilibrium solution: onset of stationary and Hopf bifurcations

For the onset of stationary convection, we consider the case $Le=2$, $\varepsilon = 0.5$, $\Psi = 0.4$ for which the results of the stability analysis, obtained either by the exact solution or the Galerkin

method, give $Ra_{cs}=12.95$ and $k_{cs}=1.94$ in an infinite layer. For $A=10$, we find numerically the critical value of the Rayleigh number: $Ra_{csnum}=13$ and the development of 6 rolls (Fig. 7) which corresponds to a wave-number in an infinite cell of $k_{Cnum} = (n\pi)/A = 1.89$ (where n is the number of convective cells).

We also study the onset of the mono-cellular flow predicted by the linear theory in a layer heated from above and for negative values of the separation ratio ψ . For $Le=2$, $\varepsilon=0.5$, $\psi=-0.2$, the linear theory gives: $Ra_{cs} = 12 / (Le\psi) = -30$, and the numerical simulation leads to $Ra_{csnum}=-32$. In Fig.8, we have plotted the streamlines, the iso-concentrations and the isotherms obtained for this case. One can observe, the deformation of the iso-concentrations which leads to a separation of the components of the binary fluid whereas the isotherms remain horizontal (diffusive thermal state).

For the onset of oscillatory convection, by studying the evolution in time of the horizontal velocity component in one point of the domain (the collocation point (10, 10)), we numerically determine the critical Rayleigh number and the pulsation corresponding to the Hopf bifurcation for the case $Le=2$, $\varepsilon = 0.5$, $\psi = -0.25$. We obtain: $Ra_{conum}=116$ and $\omega_{num}=13.75$. The Hopf pulsation is calculated from the Fourier transform of the horizontal velocity component at the onset of convection (Fig.9a and 9b). These results are very close to the theoretical ones: $Ra_{co}=114.02$ and $\omega_{co}=14.03$. Thus the relative error is 1.7% and 2 % for the critical Rayleigh number and the critical wave-number respectively. For the case studied, the solution coming from the bifurcation is unstable and the system evolves to a stationary state characterized by significant velocities and a Nusselt number (ratio of the convective heat flux to the conductive heat flux) much higher than one, showing that the Hopf bifurcation is a subcritical one. Similar results were obtained for $Le=2$, $\psi = -0.2$, $A=10$ and $\varepsilon = 0.5$. We found numerically $Ra_{conum}=95.7$, $\omega_{num}=10.57$, $kc_{num}=2.51$, while the theoretical parameters are: $Ra_{co}=95.3$,

$\omega_{co}=10.82$ and $k_{co}=2.60$ for an infinite cell. The numerical results and the theoretical ones are in very good agreement. At the onset of the oscillatory convection, we find 8 rolls (Fig. 10-a) rotating on themselves, the temperature field is pseudo conductive (Fig 10-b). This solution is not stable and evolves towards a stationary stable one. For $Le=2, \psi = -0.2, A=10$ and $\varepsilon = 0.6$ and $\varepsilon = 0.7$, we obtain respectively the critical values ($Ra_{co}=82.87, \omega_{co}=10.04, k_{co}=2.67$) and ($Ra_{co}=75.03, \omega_{co}=9.45, k_{co}=2.73$). Depending on the initial conditions introduced in the computations and on the number of collocation points (even if this number is sufficiently large), or for the same initial conditions but for different values of the normalized porosity, the stationary solution is characterized by 13, 11 or 10 rolls corresponding respectively to the values $\varepsilon=0.5, 0.6$, and 0.7 used in the computations. These stationary solutions remain stable with decreasing Rayleigh number until their corresponding turning points are reached. The turning point associated with the branch with 13 rolls is obtained for $Ra_{Tu}=64.3$, with 11 rolls for $Ra_{Tu}= 59.3$, and with 10 rolls for $Ra_{Tu}= 58.8$ (Fig. 11). By assigning the values 20 and 30 to the aspect ratio A , we obtain other branches of stationary stable solutions. The complete description of all the possible flow regimes coming from the Hopf bifurcation would require a lot of numerical simulations, which is not the main objective of this work.

For the particular case ($1 + \psi + \psi Le = 0$) we obtained the exact values of the critical parameters ($Ra_{cs}=-12(Le+1)/Le, k_{cs}=0$). For $Le = 2$, we obtained $\psi=-1/(1+Le)=-1/3$ and $Ra_{cs}=-18$. We studied this case numerically in order to corroborate the analytical results; we found the onset of convection for $Ra_{cnum} = -18.5$. The flow coming from the bifurcation is mono-cellular (Fig. 12) which corresponds to $k_{cs} = 0$.

B. Stability of the mono-cellular solution

We consider the case $Le=10$ and $\psi > 0$. We recall that we obtain a mono-cellular flow for $\psi \geq \psi_{mono} = 0.146$. For $\psi = 0.33$ the linear theory gives: $Ra_{cs} = 12 / (Le\psi) = 3.64$. In Fig.13, we plot the iso-concentrations and streamlines for $Le = 10$, $\psi = 0.33$, $Ra = 8$, and $\varepsilon = 0.5$. A mono-cellular flow is observed. Due to thermodiffusion the denser species of the mixture moves towards the cold wall at the top of the cell and the less dense species moves towards the hot wall at the bottom of the cell. The mono-cellular flow advects one of the components of the mixture towards the right part of the cavity and the other one towards the left part and leads to a horizontal stratification of the concentration field.

The linear stability of the mono-cellular flow gives: $Ra_{co2}=36.77$, $k_{co2}=2.43$ and $\omega_{co2}=5.46$ for $Le = 10$, $\psi = 0.33$, and $\varepsilon = 0.5$ in an infinite cell. Numerically, using a finite element and spectral codes for an aspect ratio $A = 10$, we observe, as the Rayleigh number increases from $Ra=3.64$, the following scenario: for $3.64 < Ra < 20$, the mono-cellular flow remains stable. For $20 < Ra < 38$, some oscillations appear at the beginning of the computation and disappear after a short time, leading to a steady mono-cellular flow. The duration of the oscillation increases as Ra increases from $Ra=20$ to $Ra=38$. For $38 < Ra < 38.5$, the oscillatory flow is maintained for all the computing times used and the frequency of the oscillations is $\omega_{co2num}=5.32$. For example, for a porous cell of 1cm height, saturated by a water-ethanol mixture, the computing time used corresponds to a dimensional time of nearly 1700 hours. We present, in Fig. 14, the time evolution of the horizontal velocity component in one point of the domain for $Ra=38$ and, in Fig. 15, the structure of the flow at three different instants of a period. For 38.6 , a steady multicellular flow takes place in the cavity (Fig. 16). For each computation and for a fixed value of Ra , the initial conditions introduced correspond to the mono-cellular ones issued from eq. 45. The relative error associated to the critical parameters is 5 % for Ra_{co2} and 2.6 % for ω_{co2} . Some computations were performed in order to analyze the influence of the aspect ratio on the critical values of the transition; we verified that the

numerical values found for the aspect ratios 10 and 50 are very close. The bifurcation from the mono-cellular flow was also studied for other values of ψ . For $Le=10$, $\varepsilon=0.5$ we obtained, for $\psi=0.2$, $(Ra_{co2}=36.61, \omega_{co2}=3.77)$, $(Ra_{co2num}=35.1, \omega_{co2num}=3.29)$, and, for $\psi=0.25$, $(Ra_{co2}=36.7, \omega_{co2}=4.5)$, $(Ra_{co2num}=36.8, \omega_{co2num}=4.33)$.

VI. CONCLUSION

In this paper, we revised and extended the problem of Soret-driven convection in a horizontal porous medium cell filled with a binary fluid. In the first part of the work, we studied the onset of Soret-driven convection in an infinite porous saturated layer heated from below or from above. The influence of a negative or positive separation ratio ψ and the importance of the role of normalized porosity, which were not taken into account by Brand and Steinberg group and by Schöpf¹³, were investigated theoretically and numerically in this paper. For stationary bifurcations and for realistic boundary conditions, an analytical dispersion relation giving the critical Rayleigh number and wave-number has been obtained for both infinite and confined cells. A very good agreement was found between the critical values obtained analytically and the ones obtained by a Galerkin numerical procedure. For Hopf bifurcations, the critical parameters depend strongly on the normalized porosity. We showed that, contrary to the result obtained by Schöpf¹³, the binary fluid convective motion in a narrow cell differs from the flow in a porous medium. Indeed in a porous medium, the thermal diffusion is effective inside the fluid and the porous matrix while the mass diffusion only operates inside the fluid.

Several numerical simulations were carried out in order to corroborate the results obtained with the linear stability analysis for the equilibrium solution. These simulations permitted us to observe the onset of many stationary subcritical convection branches and to determine the turning point associated with these several branches.

In the second part of our study, analytical and numerical techniques were used to study the stability of the mono-cellular flow obtained, for $\psi > 0$ and $\psi \geq \psi_{mono}$, when the equilibrium solution loses its stability. Direct nonlinear numerical simulations, using both a spectral collocation method and a finite element method corroborated the results of the linear stability analysis and allowed us to study the structure of the flow which appears after the bifurcation. We highlighted that the mono-cellular flow associated to a stratified concentration field leads to a horizontal separation of the chemical species of the binary mixture. This final result could be used to determine experimentally the Soret coefficient by considering the value of the critical Rayleigh number associated to the transition between the mono-cellular and multi-cellular flow. Indeed the critical temperature difference ΔT_c leading to the transition between the pure diffusive regime and the mono-cellular flow is too small to be measured with accuracy whereas the second transition, mono-cellular-multi-cellular flow, is associated with a critical temperature difference much higher than ΔT_c .

References

- ¹D. A. Nield and A. Bejan, Convection in porous media, *Springer Verlag, New-York*, 1998.
- ²D. B. Ingham and I. Pop, Transport Phenomena in Porous Media, Vol. III, Elsevier Science; Amsterdam, 2005.
- ³D. A. Nield, Onset of thermohaline convection in a porous medium. *Water Resources Res.* 4: 553-560, 1968.
- ⁴K. Vafai, Second Edition, pp 269-320, Hand-Book of Porous Media by *Marcel Dekker New York. Basel*, 2005.
- ⁵J. K. Platten and C. Legros, Convection in liquids, *Springer Verlag, Paris*, 1984.

- ⁶O. Batiste, I. Mercader, M. Net and E. Knobloch, Onset of oscillatory binary fluid convection in finite containers, *Phys. Rev. E* **59** N° 6, 6730-6741, 1999.
- ⁷H. R. Brand and V. Steinberg, Convective Instabilities in Binary Mixture in a Porous Medium, *Physica A* **119**, 327-338, 1983A.
- ⁸H. R. Brand and V. Steinberg, Non linear effects in the convection instability of a binary mixture in a porous medium near threshold, *Phys. Lett.* **93**, 333-336, 1983b.
- ⁹A. Bahloul , N. Boutana and P. Vasseur Double-diffusive and Soret induced convection in a shallow horizontal porous layer, *J. Fluid Mech.* **491**, 325- 352, 2003.
- ¹⁰M. Bourich, M. Hasnaoui, A. Amahmid and M. Mamou, Soret driven thermosolutal convection in a shallow porous enclosure, *Int. Commun. Heat Mass Transf.* **29**, N°5, 717-728, 2002
- ¹¹M. Bourich, M. Hasnaoui, M. Mamou and A. Amahmid, Soret effect inducing subcritical and hopf bifurcation in shallow enclosure filled with a clear binary fluid or saturated porous medium: A comparative study. *Phys. Fluids* **16**, N°3, 551-568, 2004.
- ¹²H. R. Brand, P. C. Hohenberg, and V. Steinberg, Codimension-2 bifurcation in binary fluid mixtures, *Phys. Rev. A* **30**, N5, 2548-2561, 1984.
- ¹³W. Schöpf, Convection onset for binary mixture in a porous medium and in narrow cell: a comparison, *J. Fluid Mech.***245**, 263-278, 1992.
- ¹⁴M. N. Ouarzazi and P.A. Bois, Convective instability of a fluid mixture in a porous medium with time-dependent temperature gradient, *Eur. J. Mech. B Fluids* **13**, 275-278, 1994.
- ¹⁵M. Quintard and S. Whitaker, Transport in chemically and mechanically heterogeneous porous media I: theoretical development of region averaged equations for slightly compressible single-phase flow. *Adv. Water Resour.***19**: 2779-2796, 1996 a.

- ¹⁶O. Sovran, M.C. Charrier-Mojtabi and A. Mojtabi, Naissance de la convection thermosolutale en couche poreuse infime avec effet Soret, *C.R. Acad. Sci. Paris* **329**, Serie Iib, 287-293, 2001.
- ¹⁷R. Bennacer, A. Mahidjiba, P. Vasseur. H. Beji and R. Duval . The Soret effect on Convection in a Horizontal Porous Domain Under Cross Temperature and concentration gradient, *Int. J. Numerical Methods Heat and Fluid Flow*.**13** (2),199-215, 2003b.
- ¹⁸A. Mojtabi, J. K. Platten and M. C. Charrier-Mojtabi, Onset of free convection in solutions with variable Soret coefficients, *J. Non-Equilib. Thermodyn* **27**, N°1, 25-44, 2002.
- ¹⁹G. Labrosse, Free convection of binary liquid with variable Soret coefficient in thermogravitational column: The steady parallel states, *Phys. Fluids* **15**, 2694 , 2003.
- ²⁰M. C. Charrier-Mojtabi, Y. P. Razi, K. Maliwan, A. Mojtabi, Influence of vibration on Soret-driven convection in porous media, *Numer. Heat transf.* **46**, 981 , 2004.
- ²¹I. I. Ryzhkov, V. M. Shevtsova, On thermal diffusion and convection in multicomponent mixtures with application to the thermogravitational column, *Physics of fluids*, **19**, 027101, 2007.
- ²²V. M. Shevtsova, D. E. Melnikov and J. C. Legros, Onset of convection in Soret Driven instability, *Phys. Rev. E*, **73**,047302, 2006.
- ²³V.M. Shevtsova, D. E. Melnikov and J. C. Legros, Unstable density stratification in binary mixture, *Progress in Computational Dynamics*, Vol. 6, N°6,348-356, 2006.
- ²⁴E. Knobloch, Oscillatory convection in binary mixtures, *Phys. Rev. A*, 2: 1538-1549, 1986.
- ²⁵M. Ouriemi, P. Vasseur, A. Bahloul and L. Robillard, Natural convection in a horizontal layer of a binary mixture, *International Journal of Thermal Sciences*, Volume 45, Issue 8, 752-759, 2006.

²⁶M. Mamou and P. Vasseur, Thermosolutal bifurcation phenomena in porous enclosures subject to vertical temperature and concentration gradients. *J. Fluid Mechanics*, 395, 61- 87, 1999.

²⁷M. Azaiez, C. Bernardi and M. Grundmann, Spectral method applied to porous media, *East-West J. Numer. Math.* 2 91-105, 1994.

		Le=2		Le=10		Le=100	
		Rac	kc	Rac	kc	Rac	kc
$\Psi=-0.1$	Exact	66.79	3.75 ₋	∞	-	∞	-
	Galerkin	66.75	3.75 ₋	∞	-	∞	-
$\Psi=-0.05$	Exact	50.12	3.41	139.46	4.83	∞	-
	Galerkin	50.13	3.41	139.00	4.82	∞	-
$\Psi=-0.02$	Exact	43.22	3.24	59.04	3.69	∞	-
	Galerkin	43.22	3.24	59.03	3.69	∞	-
$\Psi=0$	Exact	$4\pi^2$	π	$4\pi^2$	π	$4\pi^2$	π
	Galerkin	39.48	3.14	39.47	3.15	39.48	3.14
$\Psi=0.05$	Exact	32.21	2.91	19.24	2.12	2.40	0.00
	Galerkin	32.20	2.92	19.25	2.12	2.40	0.00
$\Psi=0.1$	Exact	26.99	2.72	11.68	1.28	1.20	0.00
	Galerkin	27.01	2.71	11.71	1.28	1.20	0.00
$\Psi=0.15$	Exact	23.09	2.55	8.00	0.00	0.80	0.00
	Galerkin	23.09	2.55	8.01	0.00	0.80	0.00
$\Psi=0.2$	Exact	20.09	2.40	6.00	0.00	0.60	0.00
	Galerkin	20.09	2.40	6.01	0.00	0.60	0.00
$\Psi=0.25$	Exact	17.72	2.27	4.80	0.00	0.48	0.00
	Galerkin	17.72	2.27	4.81	0.00	0.48	0.00
$\Psi=0.3$	Exact	15.81	2.14	4.00	0.00	0.43	0.00
	Galerkin	15.81	2.15	4.01	0.00	0.42	0.00
$\Psi=0.35$	Exact	14.24	2.03	3.43	0.00	0.34	0.00
	Galerkin	14.24	2.04	3.44	0.00	0.33	0.00
$\Psi=0.4$	Exact	12.93	1.93	3.00	0.00	0.30	0.00
	Galerkin	12.95	1.94	3.01	0.00	0.30	0.00

Table I. Comparison between the values of the critical Rayleigh number Rac_s and the critical wave-number kc_s obtained by the exact solution and the Galerkin method at order 4. Stationary bifurcations.

Ψ	k_{co2}	Ra_{co2}	ω_{co2}
0.15	2.60	36.53	2.81
0.16	2.58	36.54	3.03
0.17	2.57	36.56	3.23
0.18	2.55	36.57	3.42
0.19	2.54	36.59	3.60
0.20	2.53	36.61	3.77
0.21	2.52	36.63	3.93
0.22	2.51	36.65	4.08
0.23	2.50	36.66	4.23
0.24	2.49	36.68	4.37
0.25	2.48	36.70	4.50
0.26	2.47	36.71	4.63
0.27	2.46	36.73	4.76
0.28	2.45	36.74	4.88
0.29	2.45	36.75	5.01
0.30	2.44	36.76	5.12
0.31	2.44	36.76	5.24
0.32	2.43	36.77	5.35
0.33	2.43	36.77	5.46
0.34	2.42	36.77	5.57
0.35	2.42	36.77	5.68
0.36	2.41	36.76	5.78
0.37	2.41	36.75	5.89
0.38	2.41	36.74	5.99
0.39	2.41	36.73	6.09
0.40	2.40	36.71	6.19
0.41	2.40	36.70	6.29
0.42	2.40	36.67	6.39
0.43	2.40	36.64	6.48
0.44	2.40	36.61	6.58
0.45	2.40	36.58	6.68
0.46	2.40	36.54	6.77
0.47	2.40	36.51	6.87
0.48	2.40	36.46	6.96
0.49	2.40	36.42	7.06
0.50	2.40	36.37	7.15

Table II. Critical values of the Rayleigh number Ra_{co2} , the wave-number k_{co2} and the pulsation ω_{co2} for the oscillatory bifurcation from the mono-cellular flow, for $Le = 10$, $\varepsilon = 0.5$ and for different values of separation ratio Ψ (Galerkin method order 5).

List of figures

Fig. 1. : Stability diagram in the case of non realistic boundary conditions for $Le=2$, and for different normalized porosity values ($\epsilon=0.15, 0.2, 0.6, 0.8$). Solid line: stationary bifurcation, Dotted line: Hopf bifurcation, dashed line : $\psi = -1/(1 + Le)$.

Fig. 2. : Stability diagram in the case of non realistic boundary conditions for $Le=10$, and for different normalized porosity values ($\epsilon=0.15, 0.2, 0.6, 0.8$). Solid line: stationary bifurcation, Dotted line: Hopf bifurcation, dashed line : $\psi = -1/(1 + Le)$.

Fig. 3. : Stability diagram in the case of realistic boundary conditions for $Le=2$, and for different porosity values ($\epsilon=0.4, 0.5, 0.7$). Solid line: stationary bifurcation, Dotted line: Hopf bifurcation, dashed line: $\psi = -1/(1 + Le)$.

Fig. 4. : Stability diagram in the case of realistic boundary conditions for $Le=10$, and for different porosity values ($\epsilon=0.3, 0.4, 0.5, 0.7$). Solid line: stationary bifurcation, Dotted line: Hopf bifurcation, dashed line: $\psi = -1/(1 + Le)$.

Fig. 5. : Stability diagram in the case of realistic boundary conditions for $Le=100$, and for different porosity values ($\epsilon=0.3, 0.4, 0.5, 0.7$). Solid line: stationary bifurcation, Dotted line: Hopf bifurcation, dashed line: $\psi = -1/(1 + Le)$.

Fig. 6. : Stability diagram $kc_s = f(\psi)$, for $Le=10$, in the case of stationary bifurcation and realistic boundary conditions. dashed line: $\psi = -1/(1 + Le)$.

Fig. 7. : Isoconcentrations (a), streamlines (b) and isotherms (c) for $Le=2$, $\psi=0.4$, $\epsilon=0.5$ and $Ra_{csnum}=13$.

Fig. 8. : Isoconcentrations (a), streamlines (b) and isotherms (c) for $Le=2$, $\psi=-0.2$, $\epsilon=0.5$ and $Ra_{csnum}=-32$.

Fig. 9. : Onset of oscillatory convection for $(Le, \psi, \epsilon)=(2, -0.25, 0.5)$

(a) Horizontal component of the velocity at the collocation point (10, 10) versus time.

(b) Fourier transform $(Ra, \omega)_{co_num}=(116, 13.75)$, $(Ra, \omega)_{co_th}=(114.02, 14.03)$.

Fig. 10. : Onset of oscillatory convection for $(Le, \psi, \epsilon)=(2, -0.2, 0.5)$

(a) and (b) streamlines and isotherms at the onset of oscillatory convection: 8 rolls which turn on themselves, $Ra=Ra_{co}=95.7$

(c) and (d) streamlines and isotherms on the stationary branch of solution: 13 rolls, $Ra=64.5$, just before the turning point, $Nu=1.538$

Fig. 11. : Bifurcation diagram: Nusselt number versus Rayleigh number for $Le=2$, $\psi=-0.2$ and $A=10$ for two subcritical stable branches.

Fig. 12. : Isoconcentrations and streamlines for $Le=2$, $\psi=-0.33$, $\epsilon=0.5$ and $Ra=-18.5$.

Fig. 13. : Isoconcentrations and streamlines for $Le=10$, $\psi=0.33$, $\epsilon=0.5$ and $Ra=8$.

Fig. 14. Horizontal component of the velocity at the point (9, 0.3) versus time for $(Le, \psi, \epsilon, Ra)=(10, 0.33, 0.5, 38)$.

Fig. 15. : Time evolution of streamlines during a period for $(Le, \psi, \epsilon, Ra)=(10, 0.33, 0.5, 38)$. (a) : $t=570$, (b) : $t=570.5$, (c) $t=571$.

Fig. 16. : Isoconcentrations and streamlines for $Le=10$, $\psi=0.33$, $\epsilon=0.5$ and $Ra_{cnum}=38.6$.

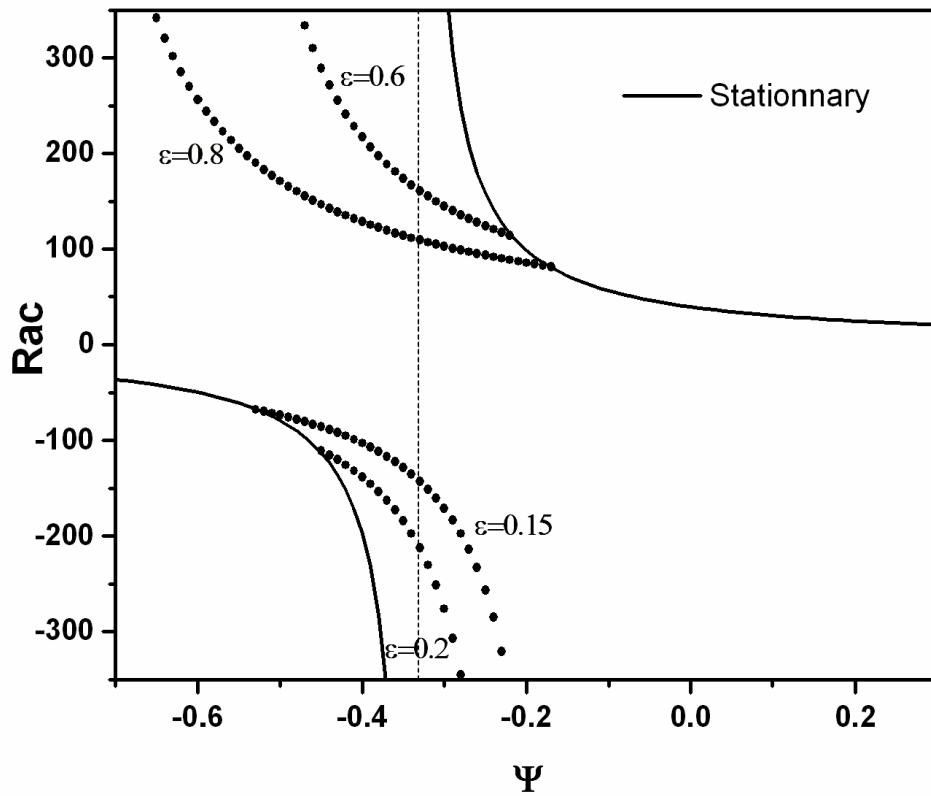


Fig. 1. : Stability diagram in the case of non realistic boundary conditions for $Le=2$, and for different normalized porosity values ($\epsilon=0.15, 0.2, 0.6, 0.8$). Solid line: stationary bifurcation, Dotted line: Hopf bifurcation, dashed line : $\psi = -1/(1 + Le)$.

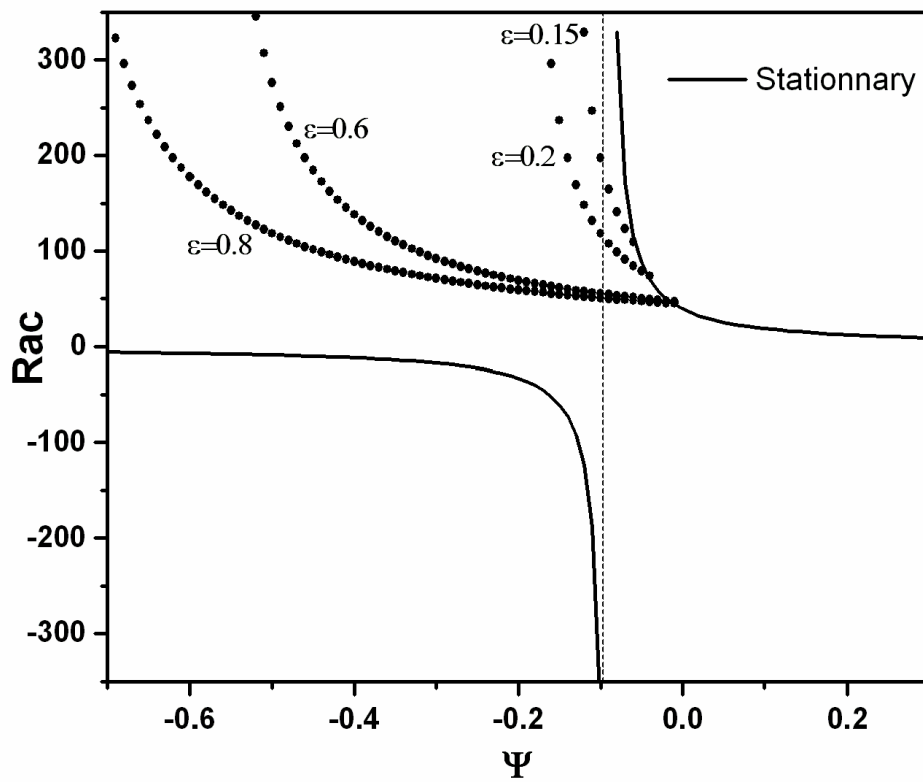


Fig. 2. : Stability diagram in the case of non realistic boundary conditions for $Le=10$, and for different normalized porosity values ($\epsilon=0.15, 0.2, 0.6, 0.8$). Solid line: stationary bifurcation, Dotted line: Hopf bifurcation, dashed line : $\psi = -1/(1 + Le)$.

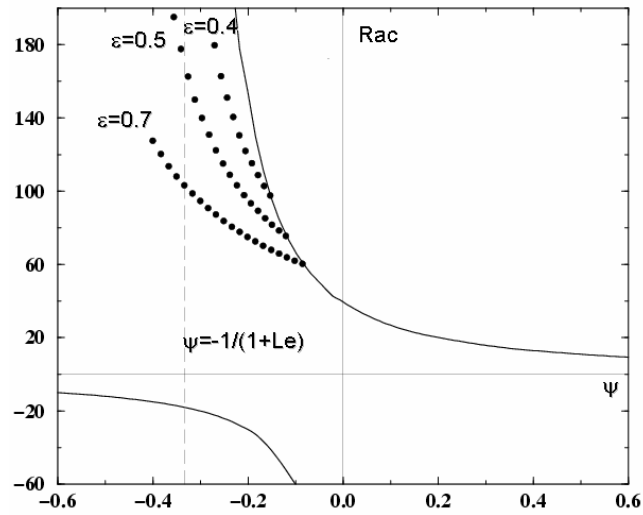


Fig. 3. : Stability diagram in the case of realistic boundary conditions for $Le=2$, and for different porosity values (0.4, 0.5, 0.7). Solid line: stationary bifurcation, Dotted line: Hopf bifurcation, dashed line: $\psi = -1/(1 + Le)$.

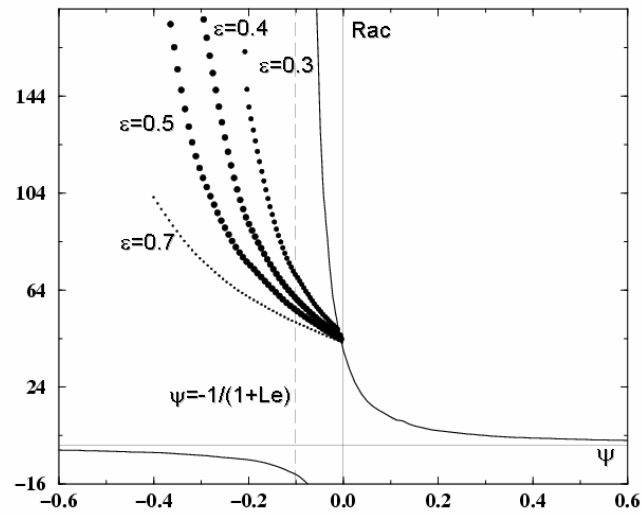


Fig. 4. : Stability diagram in the case of realistic boundary conditions for $Le=10$, and for different porosity values ($\varepsilon=0.3, 0.4, 0.5, 0.7$). Solid line: stationary bifurcation, Dotted line: Hopf bifurcation, dashed line: $\psi = -1/(1 + Le)$.

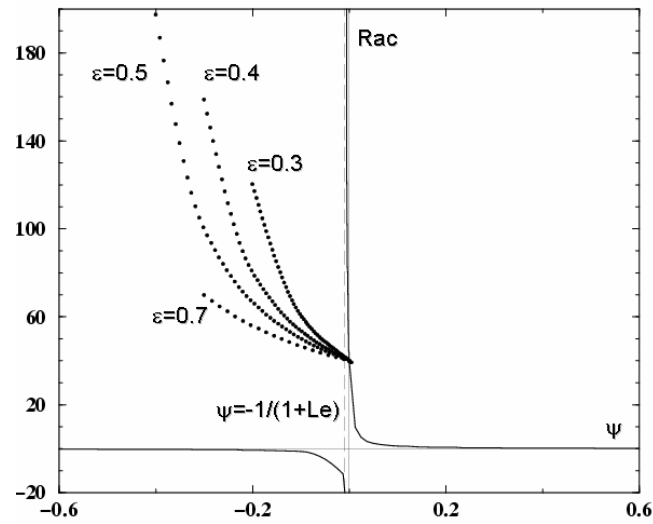


Fig. 5. : Stability diagram in the case of realistic boundary conditions for $Le=100$, and for different porosity values ($\varepsilon=0.3, 0.4, 0.5, 0.7$). Solid line: stationary bifurcation, Dotted line: Hopf bifurcation, dashed line: $\psi = -1/(1 + Le)$.

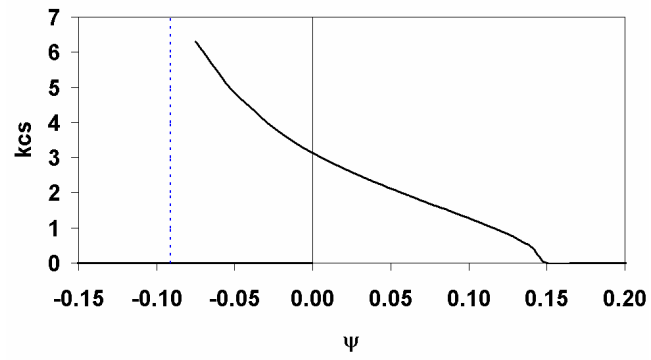


Fig. 6. : Stability diagram $kc_s = f(\psi)$, for $Le=10$, in the case of stationary bifurcation and realistic boundary conditions. dashed line: $\psi = -1/(1 + Le)$.

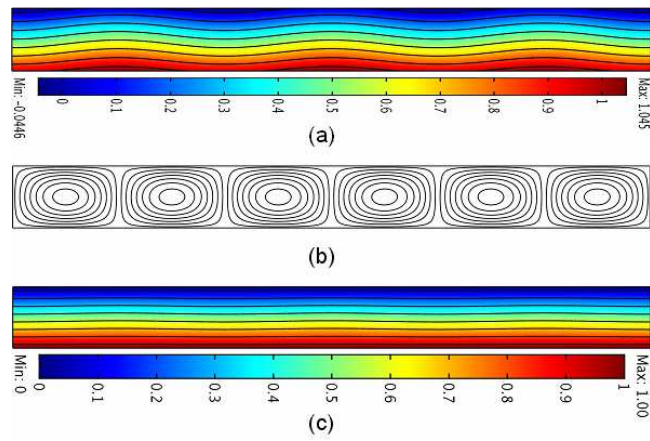


Fig. 7. : Isoconcentrations (a), streamlines (b) and isotherms (c) for $Le=2$, $\psi=0.4$, $\epsilon=0.5$ and $Ra_{csnum}=13$.

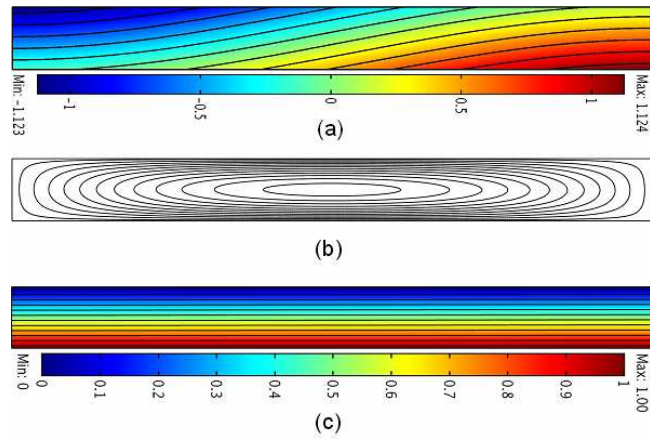


Fig. 8. : Isoconcentrations (a), streamlines (b) and isotherms (c) for $Le=2$, $\psi=-0.2$, $\epsilon=0.5$ and

$Ra_{csnum}=-32$.

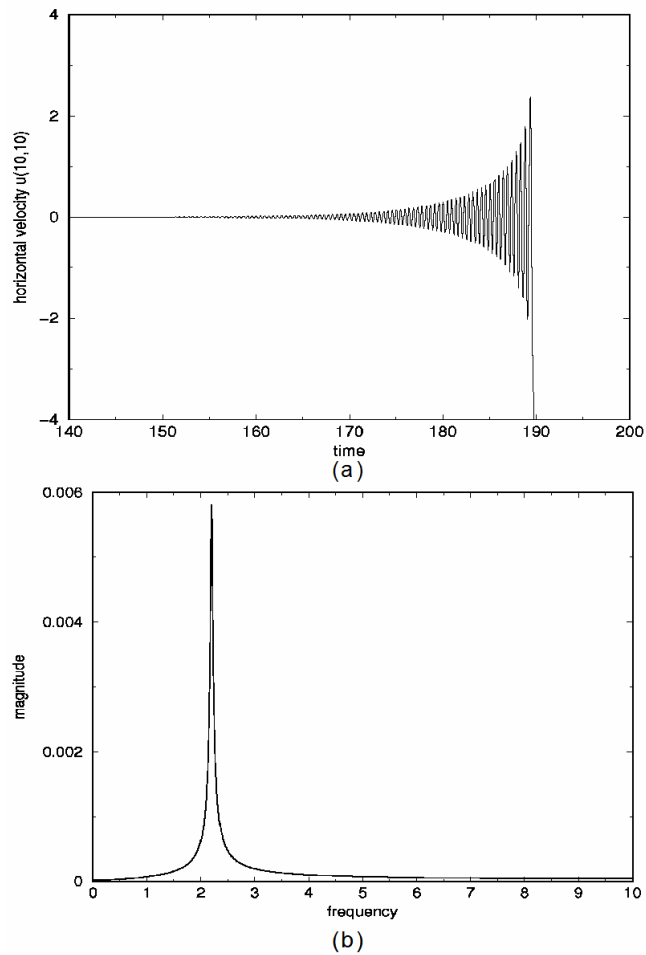


Fig. 9. : Onset of oscillatory convection for $(Le, \psi, \epsilon) = (2, -0.25, 0.5)$

(a) Horizontal component of the velocity at the collocation point $(10, 10)$ versus time.

(b) Fourier transform $(Ra, \omega)_{co\ num} = (116, 13.75)$, $(Ra, \omega)_{co\ th} = (114.02, 14.03)$.

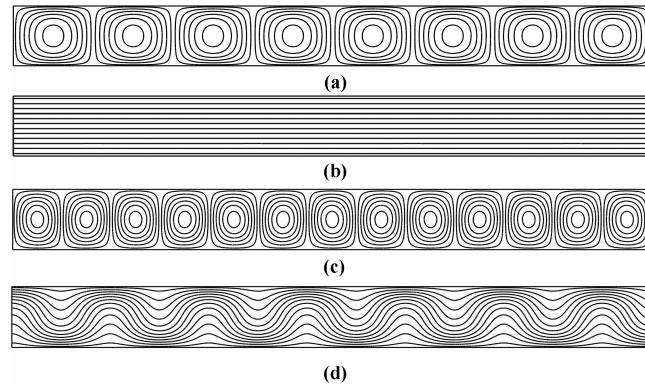


Fig. 10. : Onset of oscillatory convection for $(Le, \psi, \varepsilon) = (2, -0.2, 0.5)$

(a) and (b) streamlines and isotherms at the onset of oscillatory convection: 8 rolls
which turn on themselves, $Ra = Ra_{co} = 95.7$

(c) and (d) streamlines and isotherms on the stationary branch of solution: 13 rolls,
 $Ra = 64.5$, just before the turning point, $Nu = 1.538$

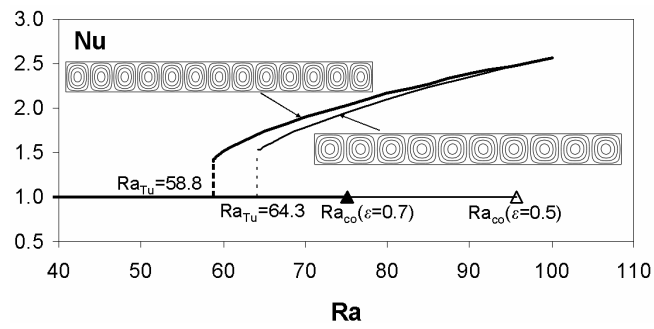


Fig. 11. : Bifurcation diagram: Nusselt number versus Rayleigh number for $Le=2$, $\psi=-0.2$ and $A=10$ for two subcritical stable branches.

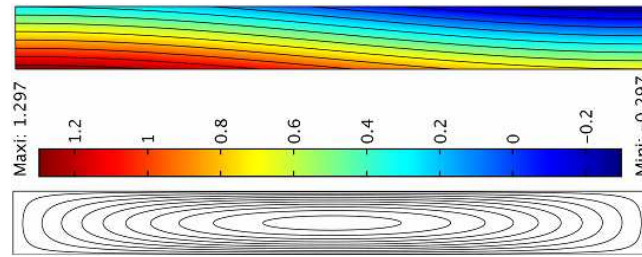


Fig. 12. : Isoconcentrations and streamlines for $Le=2$, $\psi=-0.33$, $\varepsilon=0.5$ and $Ra=-18.5$.

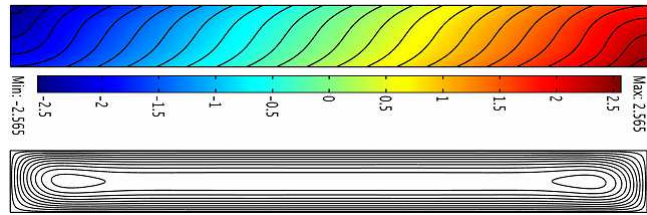


Fig. 13. : Isoconcentrations and streamlines for $Le=10$, $\psi=0.33$, $\varepsilon=0.5$ and $Ra=8$.

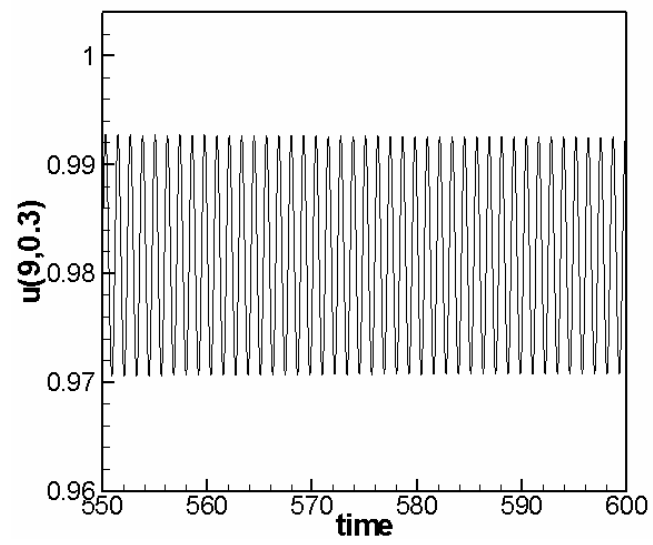


Fig. 14. Horizontal component of the velocity at the point (9, 0.3) versus time for $(Le, \psi, \varepsilon, Ra)=(10, 0.33, 0.5, 38)$.

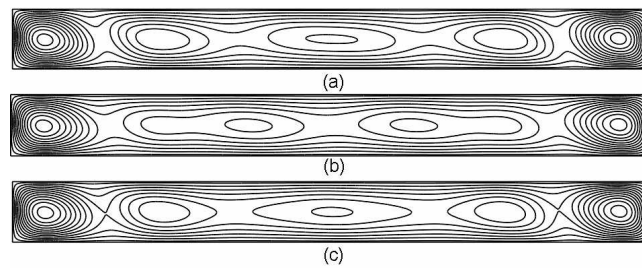


Fig. 15. : Time evolution of streamlines during a period for $(Le, \psi, \epsilon, Ra)=(10, 0.33, 0.5, 38)$. (a) : $t=570$, (b) : $t=570.5$, (c) $t=571$.

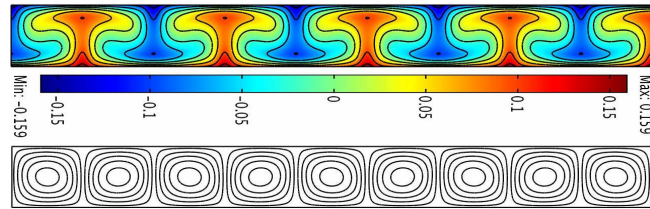


Fig. 16. : Isoconcentrations and streamlines for $Le=10$, $\psi=0.33$, $\epsilon=0.5$ and $Ra_{cnum}=38.6$.